Design and testing of a passively adaptive inlet

OPEN ACCESS
IOP Publishing
Smart Materials and Structures
Smart Mater. Struct. **27** (2018) 085019 (12pp)
https://doi.org/10.1088/1361-665X/aacf79

Design and testing of a passively adaptive inlet

G Arena[1], R M J Groh[1], R Theunissen[2], P M Weaver[1,3] and A Pirrera[1]

[1] Bristol Composites Institute (ACCIS), Department of Aerospace Engineering, University of Bristol, Bristol, United Kingdom
[2] Department of Aerospace Engineering, University of Bristol, Bristol, United Kingdom
[3] Bernal Institute, University of Limerick, Ireland

E-mail: gae.arena@bristol.ac.uk

Received 26 February 2018, revised 20 June 2018
Accepted for publication 27 June 2018
Published 11 July 2018

Abstract

Mechanical instabilities and elastic nonlinearities are emerging engineering means for designing shape-changing devices. In this paper, we exploit the taxonomy of post-buckling behaviours of a glass-fibre panel to design an adaptive air inlet that passively regulates the fluid flow into a connected duct. The adaptive component controls the inlet aperture by snapping open and closed depending on the velocity and pressure of the surrounding fluid. Sensing, actuation and control is entirely governed by the characteristics of the post-buckled component. Post-buckling stresses—induced in the composite panel by suitably applying compressive and bending loads—create the intrinsic characteristics of stability required for the panel to snap-through and snap-back. Furthermore, the associated post-buckled shape creates the aerodynamic pressure fields required for actuation. This design concept is explored and validated here by means of wind tunnel experiments. The passive actuation and control mechanism presented is particularly valuable for fluid control applications where simplicity and mass-minimisation are critical.

Supplementary material for this article is available online

Keywords: adaptive inlet, morphing structures, buckling, post-buckling, wind tunnel, design tool, elastic instabilities

(Some figures may appear in colour only in the online journal)

1. Introduction

Adaptive structures have the unique ability to change shape and/or material properties in response to varying external stimuli [1]. The application of bio-inspired adaptivity in engineering, particularly in the aerospace sector, promises significant improvements in performance—and, in turn, environmental sustainability—by making structures operate more efficiently over a broader range of operating conditions. Specifically, adaptive structures enable better trade-offs between stiffness, strength, weight and functionality [2–4]. Particularly attractive from a weight and minimal-design philosophy are *passively* adaptive structures that do not rely on separate, and often heavy, actuation devices for shape reconfiguration [5–7].

The vast majority of research on shape-changing technologies finds inspiration in nature [8]. Many organisms use adaptively compliant structures (e.g. muscles) to adapt to changing operating conditions. A fascinating example of shape-adaptability is given by the Venus flytrap, whose rapid transition from an open to a closed configuration to capture its prey occurs as the consequence of a snap-buckling instability. Specifically, the Venus flytrap uses an instability, akin to the sudden kinking of a drinking straw bent between two hands, to enable a temporary loss of structural stiffness, thereby creating the means for quick shape reconfiguration [9].

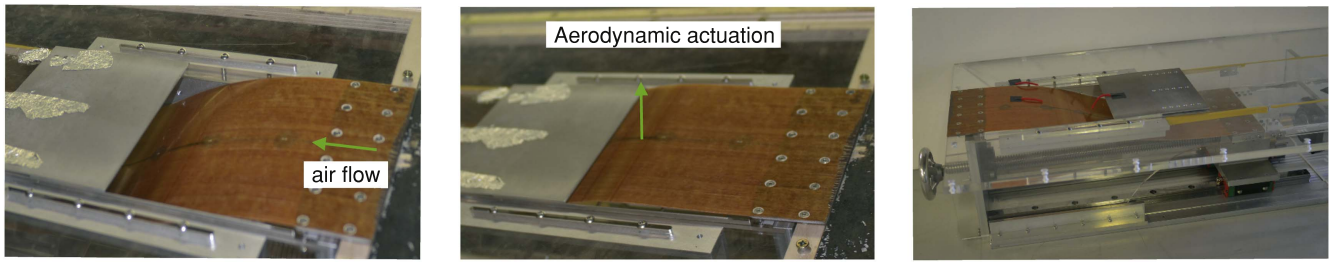

Figure 1. Adaptive air inlet demonstrator. (a) Open state. (b) Closed configuration. (c) Test rig.

The use of elastic instabilities as a means of shape adaptation has been increasingly exploited [10]. When operating conditions require large displacements and/or multiple stable configurations, structural instabilities can be viewed as a potential solution rather than—as typical in structural engineering—a source of failure [11–13]. For instance, Daynes *et al* [14, 15] manufactured a flap and an air inlet capable of snapping between two stable configurations. Both devices utilise pre-stressed composite elements for changing shape. Gomez *et al* [16] showed potential use of elastic instabilities in microfluidic applications. They demonstrated passive control of a viscous fluid flowing in a channel that involves an elastic arch. The snap-through of the arch, in this case, is passively actuated by the viscous fluid. Rothemund *et al* [17] conceived and fabricated a soft, bistable valve which acts as an air flow controller. Snapping between the downward and upward configurations is actuated by two different pressure values. Both states are also self-equilibrated, such that actuation energy is only required to switch between the states.

Tracing of equilibria deep in the post-buckling regime can reveal taxonomies of nonlinear behaviour that can then be used to design multistable snap-through responses for morphing components [18, 19]. Groh *et al* [20] recently formulated a generalised path-following technique that traces equilibrium paths on a multi-dimensional equilibrium surface of a structure defined by multiple parameters. This algorithm extends the capabilities of nonlinear finite element (FE) methods from tracing classical load-displacement paths to tracking of limit and branching points with respect to changes in geometry and/or material properties. This method enables faster exploration of the inlet's design space, since the boundaries of regions of stability, instability and multistability are readily traced in parameter space.

The taxonomy of nonlinear snap-through behaviour—explored via extensive FE and fluid-structure interaction analyses in a previous study [18]—is used here to design and manufacture an adaptive air inlet, shown in figure 1. Following a parametric exploration of the available design space by means of the methods provided in [20], dynamic FE analyses are carried out in ABAQUS in order to study the post-buckling behaviour and the fluid-structure interaction of the inlet's morphing component. The dynamic response of the air inlet to varying fluid flow conditions is then studied via wind tunnel testing.

As shown in figure 1, the inlet comprises a deformable, glass-fibre panel poised in an open state. As the air flow streaming over the panel accelerates, the changing pressure field causes the panel to snap shut at a specific velocity, thereby closing the connected duct. By careful tuning of the design parameters, the panel may remain shut or autonomously open again once the air flow falls beneath a threshold velocity. Unlike traditional shape-changing devices, the inlet does not rely on additional linkages and mechanisms for actuation, due to its inherent ability to adapt in response to external stimuli. This device has potential for engineering applications, where cooling and drag reduction create competing design drivers. Examples include air inlets on cars or cooling ducts on jet engines, where cooling with fresh air is essential for reliable engine operation but creates drag penalties at high velocities.

The remainder of the paper is structured as follows. Section 2 provides a brief theoretical background to buckling, post-buckling and the important characterstics pertaining to shape adaptation. Section 3 includes details on the FE methods and manufacturing of the test rig. Finally, section 4 discusses the multistability and aerodynamic response of the glass-fibre adaptive air inlet.

2. Theoretical background

Before delving into the details of the adaptive air inlet in section 3, this section describes, through a simplified example, the nonlinear concepts upon which the inlet design is based.

2.1. Buckling of a thin strut

The basic concepts of buckling 'failure' can be explained by considering the pin-jointed Euler strut illustrated in figure 2(a). Here, the application of a compressive axial displacement, u, initially shortens the structure in the flat configuration, but for levels of compression greater then the critical 'buckling' load, the strut suddenly deflects out-of-plane by δ, into one of the two mirror-symmetric curved configurations. Figure 2(b) shows the equilibrium branches of a perfectly symmetric system in transverse deflection versus compressive load space (often referred to as a 'pitchfork' bifurcation due to its shape). The introduction of initial imperfections that break the symmetry group along the arc-length of the strut also 'break' the pitchfork (figure 2(c)). In

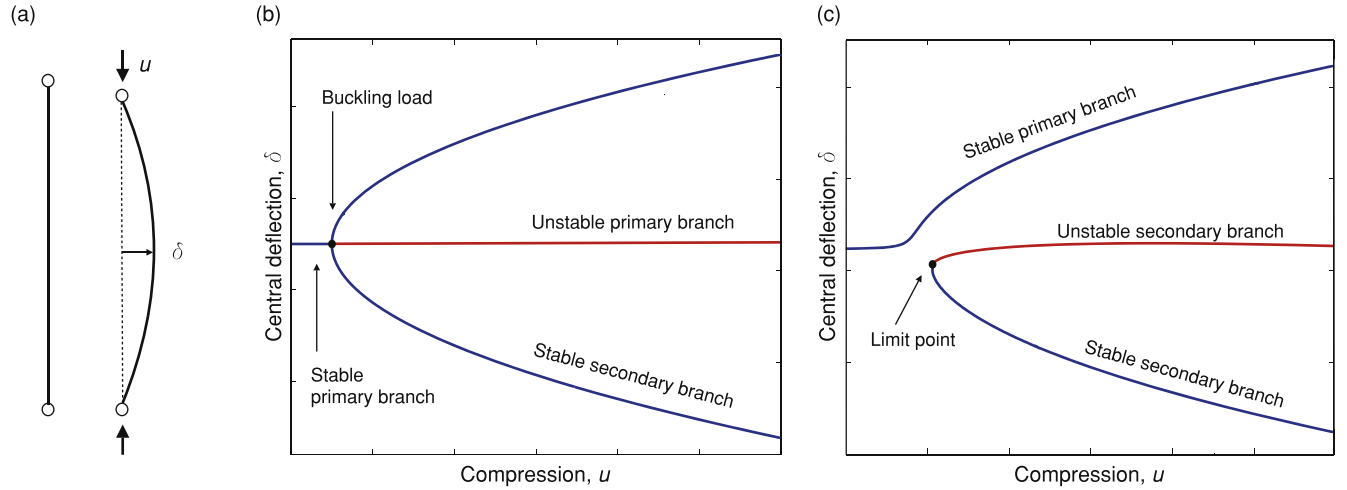

Figure 2. Buckling failure of a pin-jointed beam and corresponding bifurcation diagrams. (a) A pin-jointed beam bows sideways when subjected to a compressive force greater than the buckling load. (b) An idealised symmetric beam with no geometric or loading imperfections features a symmetric pitchfork bifurcation diagram in load versus displacement space. For small levels of compression the beam remains straight. This equilibrium destabilises at the buckling load and the structure deflects into one of two mirror-symmetric configurations. (c) Conversely, the bifurcation graph related to a beam with symmetry-breaking geometry and/or loading is characterised by a 'broken pitchfork'. It shows a primary stable branch and a secondary equilibrium branch. By applying a compressive load, the structure naturally follows the primary branch. The second configuration can be reached by application of a transverse force.

this case, as the compressive load is applied, the beam naturally follows a stable primary branch, deflecting into a preferred, bent configuration. A stable secondary branch exists and can be reached by means of an additional transverse load, F, that forces the structure to cross the solution manifold vertically, 'snapping through' a region of instability. The secondary branch of the broken pitchfork is characterised by a limit point, implying that equilibrium can either be stable or unstable depending on the magnitude of the central deflection [21].

2.2. Equilibrium paths and dynamic snap-through

A post-buckled structure is defined to be multistable when it can take two or more equilibria for the same set of external loading conditions [21]. As an example, consider the Euler strut in the inset of figure 3(a), buckled into its first stable configuration (1). For given combinations of compression and symmetry-breaking defects, such a post-buckled structure can exhibit dynamic 'snap-through' behaviour between the stable states, when subjected to an external transverse load, F. These configurations are connected by an equilibrium path, shown graphically in figure 3(a), where the magnitude of a centrally applied force, F, is plotted against the respective deflection at the midpoint, δ. The structure initially deflects in a stable manner before reaching a maximum limit point, when the strut dynamically snaps through a region of instability (2) onto the segment of the equilibrium branch to which its second stable configuration (3) belongs. Figure 3(b) shows how the equilibrium path in the F versus δ plane connects the two stable branches of the broken pitchfork. Figure 3(b) also shows how the maximum and minimum limit points of the F versus δ equilibrium path change as a function of the compressive displacement, u, by means of the black foldline.

Specifically, the foldline tracks the two limit points with respect to changes in the compressive displacement, u, thereby illustrating the border between stable and unstable equilibria. By reducing u, the two limit points of the equilibrium path in figure 3(a) gradually collide in a cusp singularity. This cusp singularity therefore determines the critical value of compression, u, at the onset of dynamic snap-through behaviour [19, 20].

The investigation of equilibrium paths and limit points provides an essential tool for using elastic instabilities as a means of shape reconfiguration [18–20]. Indeed, referring again to the canonical Euler strut, depending on the value of compression, u, three distinct types of post-buckling behaviour can be observed when the transverse load, F, is applied [18, 19]:

(i) For values of compression, u, greater than the limit point on the broken-away pitchfork branch, the structure snaps from its first stable shape to its second configuration, traversing the region of instability delimited by the foldline. A self-equilibriated second configuration exists (stable even when F is removed). The structure is said to be bistable.

(ii) Reducing the compression, u, into the region between the limit point on the broken-away pitchfork branch and the cusp singularity, allows the beam to traverse a region of instability when F is applied, thereby still exhibiting snap-through behaviour. However, at these values of compression, the structure does not have a second stable configuration for $F = 0$. This means that when the external force is removed, the strut snaps back to its primary state. In other words the structure shows 'super-elastic' monostability [19].

(iii) By decreasing the level of compression, u, even further the structure deforms nonlinearly, displaying stiffness adaptation but without snap-through. The structure is elastically monostable or simply stable.

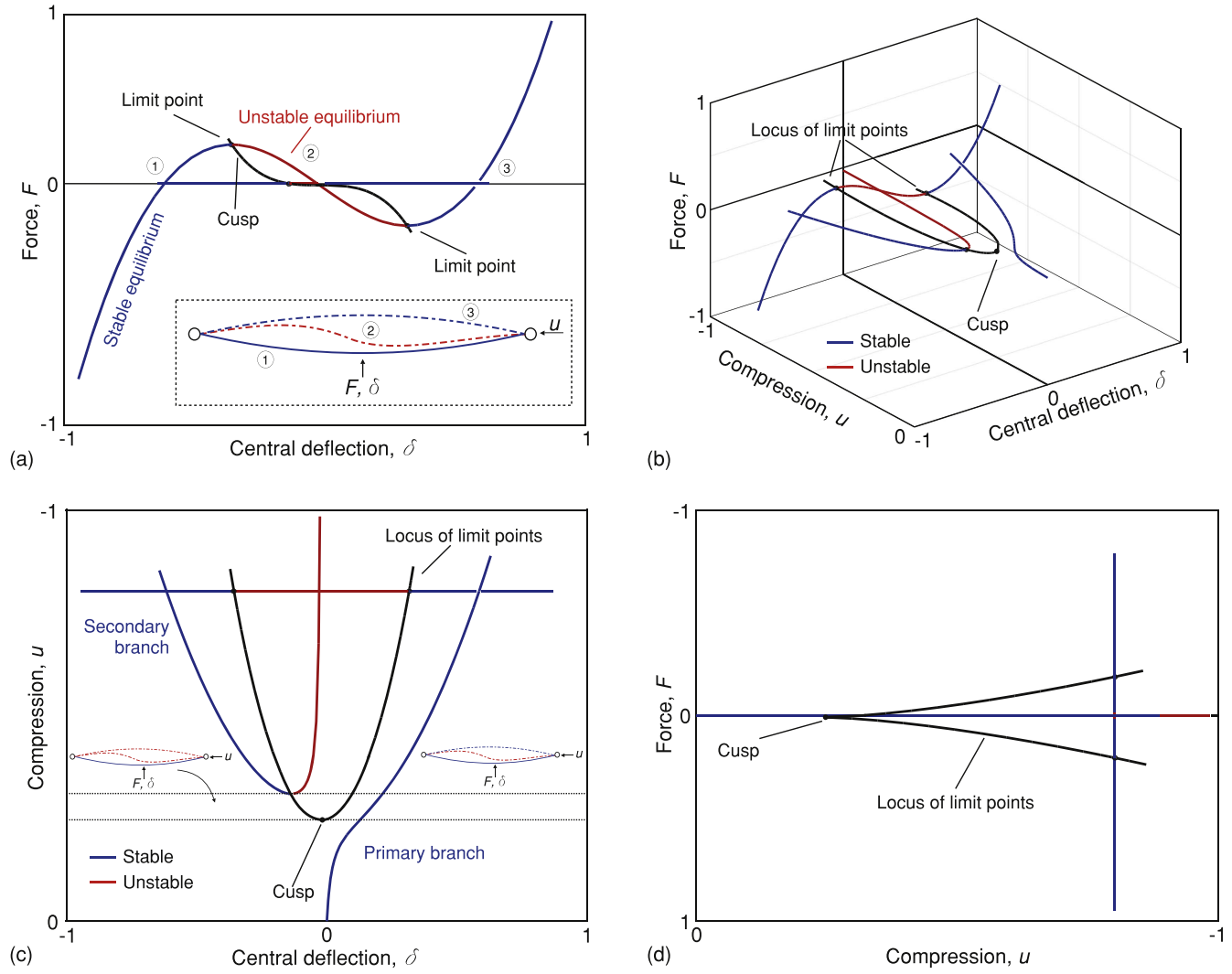

Figure 3. (a) Equilibrium path of force (F) versus central deflection (δ). (b) Compression-central deflection-force space showing a broken pitchfork and the locus of limit points of the snap-through curve. Panels (c) and (d) show the locus of limits point in central deflection-compression and compression-force space, respectively. (All curves computed using the generalised path-following framework of Groh *et al* [20].)

The mechanical instabilities of any structure can be investigated in order to define such a taxonomy of possible nonlinear behaviours, and this design space then exploited for shape-adaptability. The control of geometrical parameters, material properties and/or boundary conditions can be used to tailor the equilibrium manifolds in order to modify and adapt multistability of the system to specific working and environmental conditions [18, 20].

3. Methods

As mentioned in section 1, we study and tailor the dynamic response of a glass-fibre composite panel that can dynamically snap between two configurations and be used as the morphing component of a passively adaptive air inlet. By varying the layup sequence and boundary conditions of the composite panel, any of the three behaviours discussed above can be achieved. The nonlinear behaviour of the morphing component and aerodynamic response of the air inlet to various fluid flow conditions are tested in a sub-sonic wind tunnel available at the University of Bristol. Snap-through and snap-back trends are compared with numerical results obtained from ABAQUS simulations.

Linear structures are typically designed to specifications that define a particular geometry and loading environment. In an optimisation study the material properties can, for example, be tailored to guarantee safe operation for minimum mass. In the case of multistable nonlinear structures the specifics of the loading environment are initially not as important. In contrast, it is critically important to ensure that the structure can snap and be mono- or bistable. The particulars of the loading environment change the shape of the snap-through equilibrium curves (limit points and cusps), but the qualitative aspects of the bifurcation diagrams themselves remain unchanged. Hence, the characteristics of stability of the system are not influenced by the type of load used to switch between stable configurations, because these equilibria

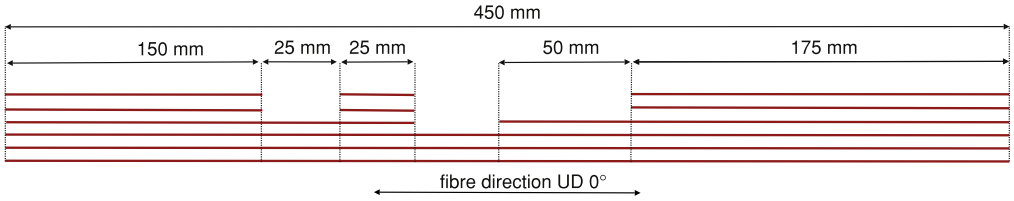

Figure 4. Composite layup for the multistable component. Red lines represent composite layers. Step changes in thickness cause stiffness variations and the structural asymmetry required for monostable behaviour with snap-through.

Table 1. E-Glass 913 layer properties.

Material	Density	Tensile modulus E_1 (GPa)	Tensile modulus E_2 (GPa)	Thickness (mm)
E-Glass 913	1900	38.7	15.4	0.125

are inherent properties of the system that exist in the unloaded state [18]. This feature allows a different design approach to be followed that focuses on the qualitative aspects of the structure first (without focusing on details of the load), with subsequent design refinement afterwards (including details of the load). This is particularly attractive for this study, as most of the optimisation can be performed in a quasistatic setting first, and then the design can be refined in a more computationally intensive fluid-structure interaction step.

3.1. Abaqus structural model

A FE model of the adaptive component of the air inlet is constructed. The material chosen is a uni-directional (UD) glass-fibre epoxy resin composite, E-Glass 913, with material properties as shown in table 1. In order to induce not only bistability, but also super-elastic monostable snap-through behaviour, the symmetry of the structure is broken by changing the thickness along the length of the panel, as shown in figure 4. With reference to the geometry of the demonstrator in figure 1, the layup sequence is also chosen as a result of a parametric study to obtain a buckled configuration that is flush with the external aerodynamic surface of the air inlet and to maximise the duct aperture. Although a simpler layup is possible to guarantee super-elastic monostability, the chosen layup and variable stiffness is driven by aerodynamic requirements on the actuated and unactuated shapes. The structure is therefore composed of a minimum of three and a maximum of six layers, where each layer has a thickness of 0.125 mm, a maximum length of 450 mm and a width of 150 mm. Vertical displacement and precompression are applied to the last 50 mm of the right end of the composite plate. The vertical displacement is kept at 50 mm, while precompression varies from 0 to 10 mm. The second equilibrium configuration is reached by application of concentrated transverse forces acting on the central nodes across the width of the plate.

Four-noded doubly curved shell elements with reduced integration S4R and enhanced hourglassing control are selected for the ABAQUS simulations. A fine mesh with 6720 elements is required to ensure convergence in the nonlinear post-buckling behaviour. Equilibrium manifolds in transverse central deflection versus compression space, as well as transverse load versus transverse central deflection snap-through curves are traced numerically by means of the ABAQUS implementation of the arc-length method based on Riks' formulation [22].

3.2. Wind tunnel experiments

Alongside the ABAQUS FE model, experiments in the low turbulence wind tunnel at the University of Bristol are carried out to investigate the inlet response to varying fluid flow conditions. The wind tunnel has an octagonal working section of 0.8 m × 0.6 m × 1 m and can attain speeds up to 88 m s^{-1} while maintaining turbulence intensity levels in the order of 0.09% due to its 12:1 contraction ratio.

An adaptive air inlet, schematically shown in figure 5, was designed and manufactured as illustrated in figure 6. The main component consists of a multistable composite plate designed using the FE buckling and post-buckling study described in section 3.1. The composite plate is composed of three to six plies of conventional E-Glass 913 reinforced epoxy matrix UD prepreg (HexPly 913G-E-5-30), with 0.125 mm of nominal cured thickness, and mechanical properties as show in table 1. A UD panel, with ply sequence as per the scheme of figure 4, cured with a vacuum-bagging technique at a temperature of 125 °C and pressure of 1 bar for 60 min. A heat-up rate of 2 °C min^{-1} was chosen. The cured panel was cut with a diamond blade to obtain a width of 150 mm and length of 450 mm, of which 50 mm are clamped on each side of the air inlet mechanism as shown in figure 6, resulting in a final length, L, of 350 mm.

Figures 6(b)–(d) show in detail the mechanism and connected components used to apply the vertical displacement and precompression necessary to buckle the composite panel and achieve the desired post-buckling behaviour. One extremity of the composite plate (1) is clamped to a 10 mm thick Polymethylmethacrylate (PMMA) plate, which is bolted on the floor of the wind tunnel. The other end of the inlet is connected through an opening in the PMMA plate to an aluminum support (9) placed immediately underneath the wind tunnel floor. With this arrangement, the height difference between the extremities of the composite panel is exactly 50 mm. Compression is imposed by a simple linear mechanism: the handwheel's (5) rotation applies torsion to a TR 20 × 4 D steel trapezoidal

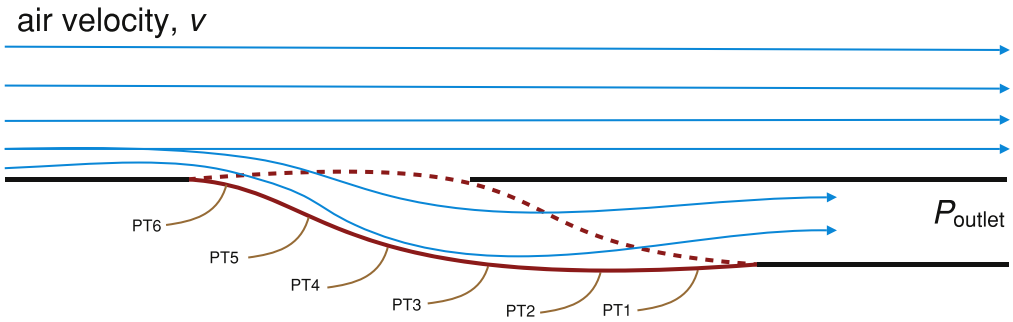

Figure 5. Schematic of the adaptive inlet and six pressure taps (PT) located along the composite plate. Dashed red line represents the closed configuration of the morphing component.

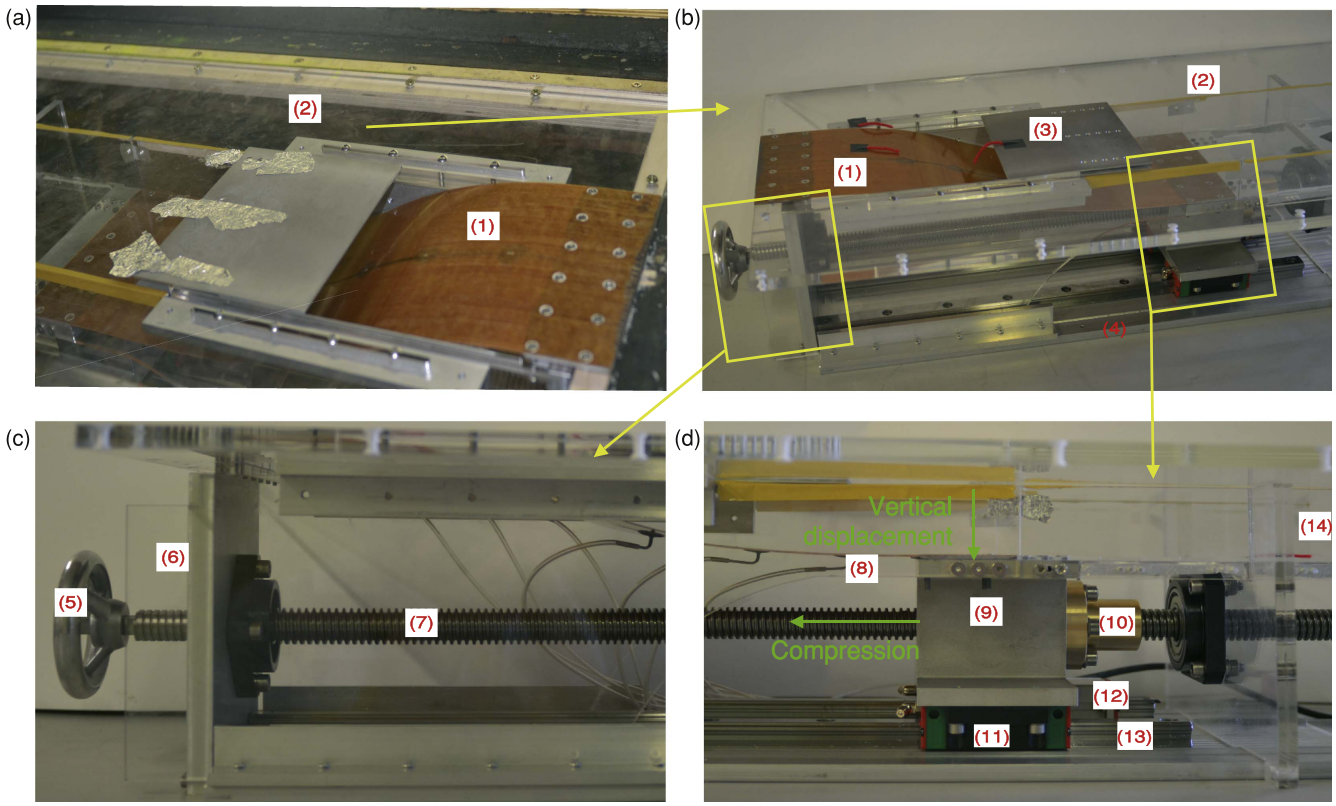

Figure 6. The air inlet placed in the wind tunnel. (a) One of the composite panel's extremities is clamped to the PMMA plate on the wind tunnel floor. Air flows through the duct to the bottom of the tunnel. (b) The full test rig is shown with details in (c) and (d). The mechanism is composed of: (1) morphing composite inlet; (2) PMMA plate; (3) adjustable cover tap; (4) aluminum bottom plate; (5) handwheel; (6) PMMA lateral walls; (7) trapezoidal lead-screw; (8) pressure taps; (9) aluminum right support; (10) bronze trapezoidal flanged nut; (11) Hiwin carriage; (12) encoder for linear measuring system; (13) Hiwin linear rails; (14) outlet channel.

lead-screw (7) that converts rotational motion to linear displacement by means of a KSM 20×4 bronze flanged trapezoidal nut (10) fixed to the aluminum support for the composite panel. A controlled and smooth linear movement is guaranteed by the HIWIN HGW20CCZ linear carriages (11) and HGR20RH-500 rails (13) on which the support is fixed. Compressive displacement is measured by the encoder (12) of an HIWIN MAGIC PG positioning measurement system. The lead-screw, nut, support bearings and HIWIN linear systems were purchased from MOORE INTERNATIONAL LTD. PMMA lateral walls (6) are abut the composite panel on both sides in order to drive the air flow above its surface and to allow the air to flow out and through an outlet channel (14) of 200 mm in length. The manufactured air inlet is placed on the floor of the working section of the wind tunnel.

During wind tunnel testing, the inlet is initially set into its open configuration. This stable post-buckled configuration is achieved by applying a compressive displacement at the lower edge of the plate. A range of displacements from 3.6 to 6 mm is applied and, for each value, the test is repeated 5 times. This provides the best data independency with uncertainty levels (at 95% confidence) less than 10% of the velocity and pressure at snap-through.

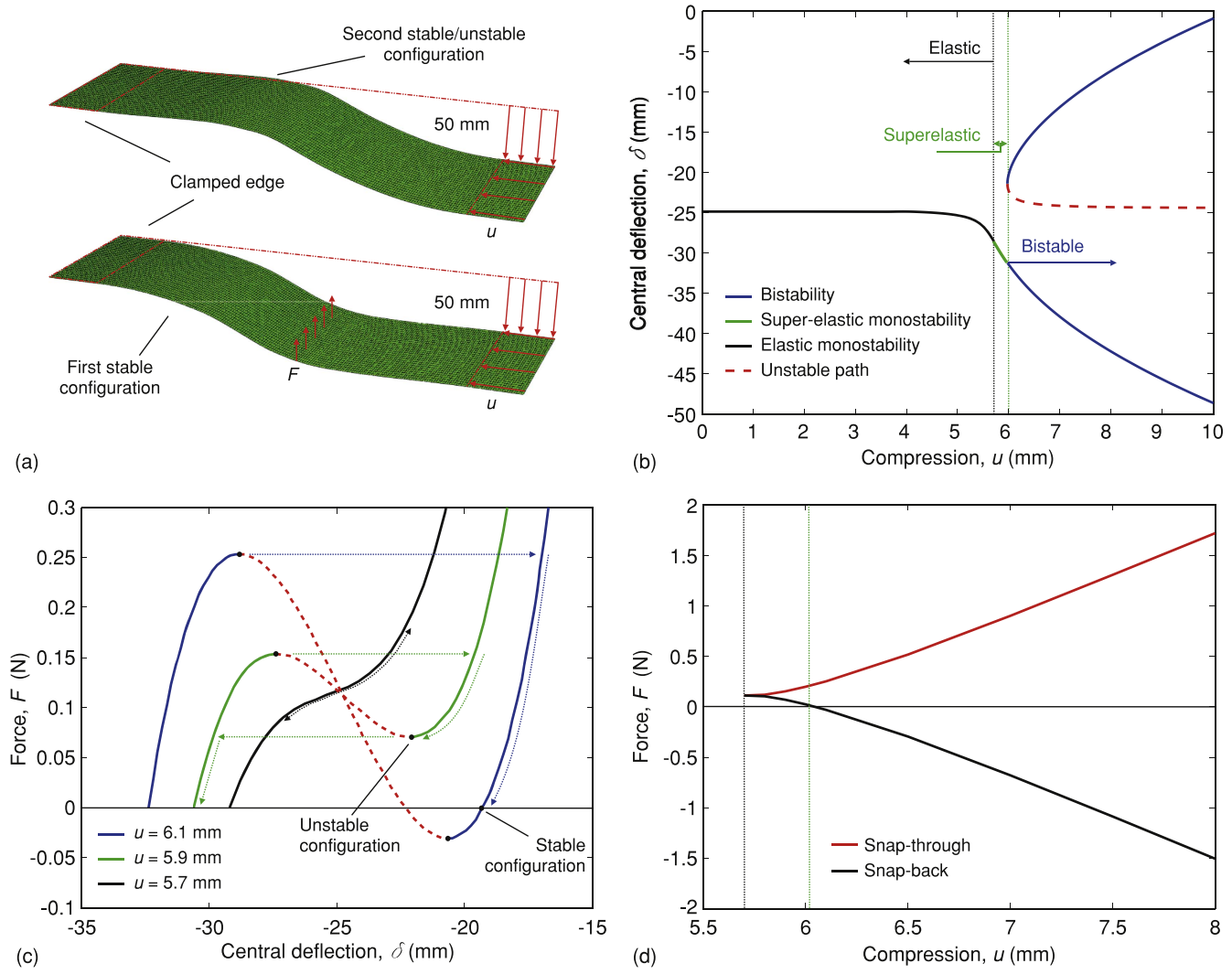

Figure 7. Finite element buckling analysis of a multistable composite plate. (a) First and second buckling configurations of the morphing component. (b) Broken pitchfork in compression-central deflection space and related dynamic behaviour. (c) Snap-through curves of a bistable, super-elastic monostable and simply stable structure. (d) Locus of limit points in compression-force space.

The initially stable shape of the composite plate corresponds to the maximum inlet aperture. The morphing panel then snaps onto its second equilibrium as the fluid velocity is increased and reaches a critical value, thereby closing the inlet. The second state can either be self-equilibrated, meaning that the inlet will remain closed even when the air ceases to flow (bistability), or super-elastic, i.e. the plate returns to its open configuration once the fluid flow speed is reduced.

The structural behaviour of the morphing component is studied by recording the static pressure profile induced by air flowing over the structure. Six pressure taps are placed on the back side of the composite plate (figure 5) and connected to a MicroDaq Pressure Scanner. The pressure taps for the pressure distributions were made from 1.6 mm diameter brass tubing with 0.4 mm pinholes with angle perpendicular to the surface of the composite plate to avoid aerodynamic interference between the pressure taps. Each of these taps measure pressure relative to the atmospheric value, for 50 s, at a frequency of 1000 s^{-1}. Additionally, total and static pressure taps of a Pitot tube, placed inside the wind tunnel, were connected to the pressure scanner. Using Bernoulli's equation

$$P_{\text{tot}} - P_{\text{stat}} = \frac{1}{2}\rho v^2 \tag{1}$$

the pressure data from the Pitot tube was used to calculate the instantaneous air flow velocity in the wind tunnel, v, for a specific density $\rho = 1.225\ \text{kg m}^{-3}$ of the fluid, and where P_{tot} and P_{stat} are total and static pressure, respectively.

4. Results

The results of the ABAQUS study are summarised in section 4.1 before the experimental wind tunnel results are then presented in section 4.2.

4.1. Design of the multistable component

Figure 7 summarises the results obtained from the buckling and post-buckling study of the glass-fibre structure. As shown

in figure 7(a), the composite plate is clamped at its left extremity, while the application of 50 mm of vertical displacement and compression, u, to the right extremity produces the first buckled stable configuration. The second state is reached by loading the structure via a transverse load. Depending on u, this configuration can be either stable or unstable. Because the composite plate contains asymmetries in its geometry, the pitchfork equilibrium manifold is broken, as shown in figure 7(b). When u is applied, the structure naturally follows the primary equilibrium branch and at $u \approx 5$ mm it deflects into its initial 'open' configuration with negative central deflection. Note that before compression, the central deflection is approximately -25 mm. This is due to the vertical displacement of the right extremity of the plate, which is applied as a initial loading step before compression.

The findings of the post-buckling study provide general guidelines for designing the adaptive air inlet. The dynamic response and multistable capabilities of the composite panel are summarised in figures 7(b)–(d). Starting from a constant value of $u = 6.1$ mm, which is beyond the limit point on the broken-away pitchfork branch of the bifurcation diagram of figure 7(b), the snap-through equilibrium curve in figure 7(c) shows that the structure snaps through into its second configuration when F reaches 0.25 N. If the transverse load is removed, the structure remains in the inverted position at the point where the load-displacement curve intersects the zero-force axis. A force of -0.025 N is required to snap back to the first state. In conclusion, for values of compression greater than the limit point of the broken-away pitchfork branch, the structure behaves in a bistable manner. In this configuration, the midpoint of the composite can deflect up to 50 mm for $u > 10$ mm.

By reducing the compressive displacement to $u = 5.9$ mm, the structure lies in the super-elastic zone between the limit point on the broken-away pitchfork branch of figure 7(b) and the cusp of figure 7(d). With reference to figure 7(c), the green fundamental path shows that after snap-through at around $F = 0.15$ N, the structure reaches a second configuration. This state is unstable and the composite panel automatically snaps back upon load removal.

Figure 7(d) shows the cusp singularity on the locus of limit points on snap-through deflection (δ) versus load (F) curves. The red curve represents the forces at which the panel snaps through (locus of maxima) onto the second equilibrium, while the black curve shows the forces at which the panel snaps back (locus of minima), both as a function of u. As previously described in section 2, the cusp defines the onset of snapping behaviour. Consequently, no snap-through is observed if the system is configured to have a compressive displacement below the cusp value. The region of super-elastic monostability is confined between the cusp and the intersection of the snap-back curve with the compression axis $F = 0$.

4.2. Wind tunnel experiment

The results illustrated in section 4.1 show the taxonomy of dynamic snap behaviour of the UD glass-fibre composite panel under consideration. In a recent fluid-structure interaction (FSI) study, Arena *et al* [18] demonstrated that an air inlet, designed using this taxonomy, can be actuated by aerodynamic loads when air flow reaches a critical speed. The fluid flow conditions above the curved morphing component applies a field of negative relative static pressure distributed across the composite surface, which pulls the structure up and actuates the snap-through.

In this section, we present an the experimental validation for this design principle for the development of shape-adaptive devices. Specifically, the inlet's dynamic response to varying airspeed is tested throughout wind tunnel experiments.

The air inlet was designed to remain open for slow fluid flows and to close immediately when the airspeed reaches a critical value. For this reason, the composite component is designed to always buckle into the 'open' configuration upon compression, such that it can then be snapped into the 'closed' state.

It is important to note that the experimental values of compression reported here are generally lower than those obtained with the FE investigation (figure 7), because the calibration of the positioning measuring system cannot be done with the composite component in its completely undeformed, straight configuration. In addition, it is also noted that deviations from previous FSI calculations [18] are expected, because the aerodynamic loads acting on the structure are influenced by turbulence generated by edges and imperfections. Therefore, the structural behaviour outlined by means of FE and FSI analyses can only be compared qualitatively with the experimental results.

As described in section 3.2 and figure 6, the top PMMA plate of the test rig was placed flush with the wind tunnel floor, whereas the rest of the mechanism is fixed underneath.

Figure 8(a) shows the adaptive inlet in its open configuration. For values of $u \geqslant 4.4$ mm, the structure shows bistability. In particular, for airspeeds greater than $v = 31.7\ \mathrm{m\,s^{-1}}$, and relative pressure (pressure difference with respect to the atmospheric one), $P = -202.0$ Pa, the structure snaps into its closed configuration (figure 8(b)), which remains stable even when the velocity is lowered below these values. When the applied compressive displacement is reduced to values below 4.4 mm, the second closed configuration becomes unstable. Hence, the composite panel snaps back, and opens the inlet again, once the airspeed falls below a critical value. Both the bistable and super-elastic inlet's configurations are shown in see SI video 1 available online at stacks.iop.org/SMS/27/085019/mmedia.

In order to quantify the critical velocities and pressures at snap-through and snap-back, relative static pressure was measured along the composite panel, as shown in figure 5. An example of the extrapolated results is illustrated in figures 9(a) and (b), for a bistable and monostable configuration, respectively. A negative pressure implies the local static pressure to be inferior to the atmospheric one, essentially indicating the presence of a force normal to the composite panel and directed into the airstream. The figure shows the static pressure at the leading (PT6) and trailing (PT1) edge of the

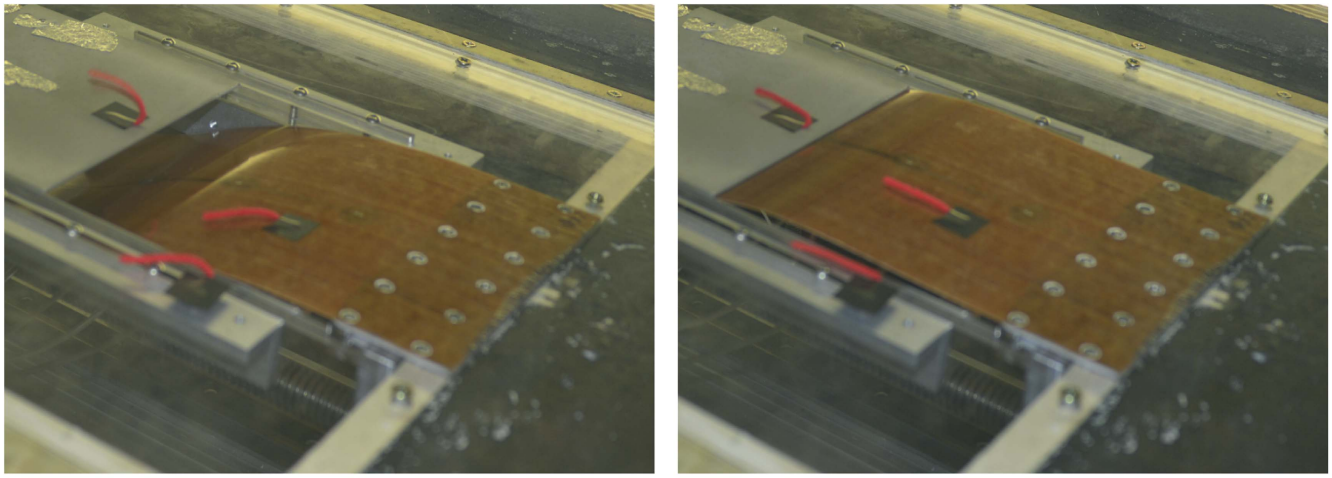

(a) (b)

Figure 8. Adaptive air inlet in its (a) open and (b) closed configuration.

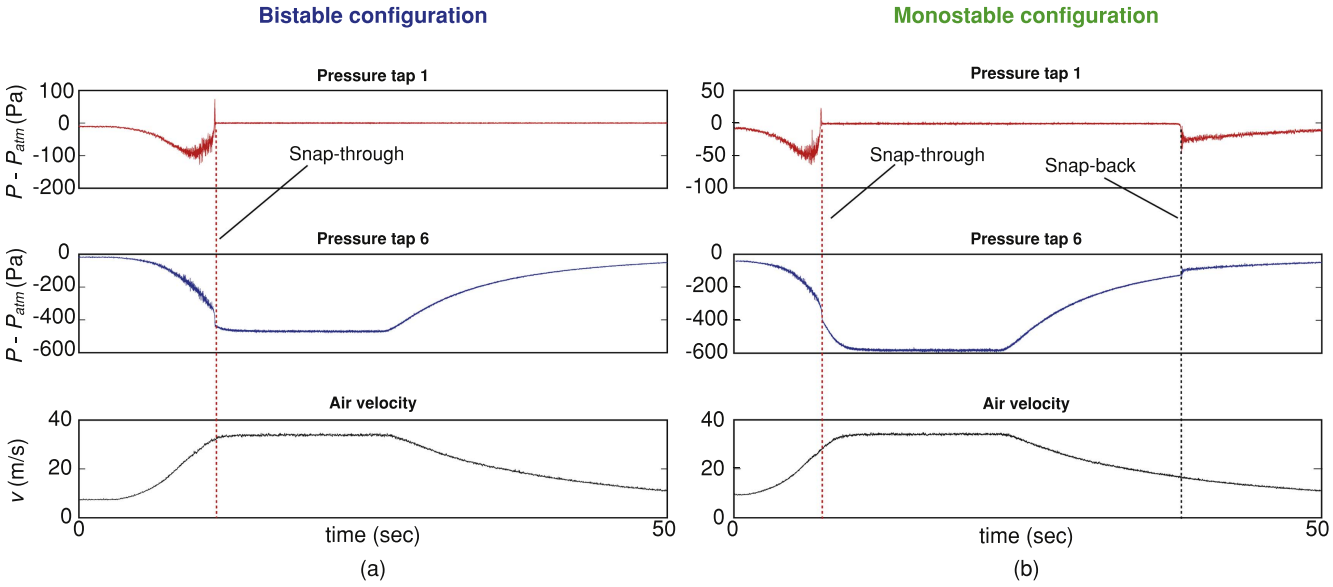

Figure 9. Measurement of relative static pressure of PT1 and PT6 and airspeed for (a) bistable and (b) monostable configurations.

composite plate, as a function of the measurement time. Both pressure curves clearly indicate when the structure snaps between open and closed states, thereby providing critical pressure and critical velocity at snap-through and snap-back. The blue curves related to PT6 show that, with an increase in air velocity, the pressure smoothly decreases until snap-through occurs, modifying the curvature of the structure and causing a sudden jump in pressure. PT1 also indicates an initial decrease in relative pressure. In this case, on the left-hand side of the critical snap-through speed, PT1 records more chaotic pressure changes. This is because the trailing edge of the composite plate vibrates just before snap-through, contributing to the formation of turbulent flow and alternating pressure changes. Nonetheless, snap-through is still clearly visible from PT1 measurements because, as the inlet closes, air ceases to flow through the air duct and the relative pressure instantaneously drops to zero. When the inlet is configured to be bistable, decreasing the air velocity does not alter the relative pressure at PT1 (which it is shielded from the air flow in the duct), while PT6 shows that the relative pressure reduces without any discontinuities associated to snap-back. Conversely, figure 9(b) illustrates clearly that when airspeed is reduced below a critical value, the actuation of the snap-back causes the inlet to re-open. Consequently, the relative pressure in the proximity of PT1 reduces again and the PT6 curve shows an additional jump. Critical values of pressure and velocity are therefore indicated by jumps in the pressure measurements.

At snap-through, the red curves in figure 9 show a peak of positive pressure. This can be related to a fluid hammer [23], similar to those commonly experienced in pipeline systems. Due to the dynamic closing of the inlet, the air flow

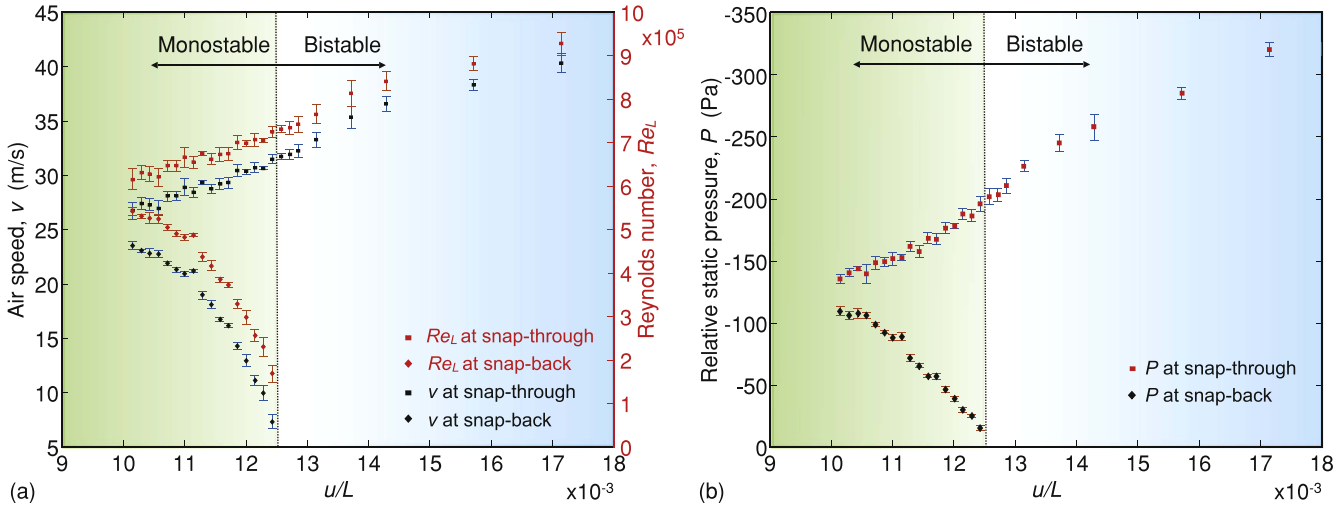

Figure 10. Non-dimensional compression, u/L, as a function of (a) airspeed, v, (left y-axis) and Reynolds number, Re_L, (right y-axis) and (b) relative static pressure, P, measured from PT5. Squared markers represent the values at snap-through, whereas diamonds represent the values at snap-back.

is suddenly forced to stop, causing a pressure wave that, in this case, is dissipated without influencing the structural behaviour of the composite component.

The dynamic response of the adaptive device is summarised in figure 10, where the non-dimensional compression, u/L, is plotted as a function of critical pressure, critical velocity and corresponding Reynolds number, RE_L. The latter is calculated with air properties at standard temperature and pressure, and the length of the morphing element (L) is chosen as the characteristic length. Error bars correspond to the 95% confidence level based on a Student's t-probability distribution for the five test repetitions considered. For values of u/L between 12.6 and 17.1 $\times$ 10^{-3}, velocities between 31.7 and 40.3 m s^{-1} (or, equivalently, pressures between -202.0 and -320.3 Pa) are required to actuate snap-through and close the air inlet. In this configuration, the inlet is bistable and maintains its closed state when airspeed is decreased to 0 m s^{-1}.

Lowering the compression to 12.4 $\times$ 10^{-3}, the inlet starts to show super-elastic monostability. In particular, at this level of compression, air flow has to reach a velocity of 31.5 m s^{-1} in order to actuate snap-through and close the inlet, whereas the velocity must be reduced to 7.2 m s^{-1} to open it again. The lower the compression, the lower the velocity (or pressure) gap between snap-through and snap-back.

With reference to figure 7(d), the curves in figure 10 show a qualitatively similar trend. The loci of maxima and minima seem to coalesce in a cusp singularity. However, for low values of compression, the influence of turbulence and the presence of the inlet cover, make the identification of the limit points highly sensitive to noise. The gaps in pressure from graphs like figure 9 become undetectable at lower values of compression.

The results obtained from the wind tunnel experiments demonstrate the flexibility of this device. By simply changing one design parameter, in this case the compression, the device can be adapted to a wide range of working conditions.

5. Discussion and conclusions

Structural adaptivity is an enabling concept when an engineering system requires trade-offs between stiffness, strength, weight and functionality. Mechanical instabilities are emerging as an effective and promising means for shape adaptation. Furthermore, current research is focusing on identifying different types of nonlinear structural behaviour from the study of equilibrium manifolds that can be used for novel functionality.

In a previous publication, Arena *et al* [18] investigated the influence of boundary conditions and geometrical parameters on the multistability and snap-through responses of a simple beam. A taxonomy of nonlinear dynamic behaviours was classified, which is used herein to design and test a shape-adaptive air inlet. The device is able to morph in response to external stimuli. In particular, the inlet is conceived to be open at low airspeeds, such that air can flow freely into a connected duct. When the airspeed increases above a predefined critical value, the adaptive component—a glass-fibre composite plate—snaps passively and closes the inlet to the duct, so that air ceases to flow into the channel. Depending on the boundary conditions applied on the composite panel and its stiffness profile, the air inlet can either remain in its closed state or autonomously snap back and open again when the airspeed reduces. External mechanisms are therefore not required for the snap-through actuation as this is driven by external stimuli instead.

The first stage of the inlet development begins with an FE analysis of the buckling and post-buckling behaviour of the glass-fibre composite plate. The choice of composite material stems from the advantage of obtaining a thin, lightweight

structure. In addition, composite manufacturing techniques, such as layup vacuum-bagging and potentially, in the future, tow-steering [24, 25], allow local tailoring of the material stiffness and the equilibrium manifold.

Wind tunnel tests have been performed to validate the proposed design concept and investigate a variety of responses to changing airspeeds. The information gathered from the FE study is used to manufacture a test rig. The taxonomy of adaptive behaviours is verified by investigation of the critical velocity and static pressure at snap-through and snap-back as a function of the applied compressive displacement on the shape-changing composite panel. The control of this parameter, through a system comprising a lead-screw and linear rails, successfully permit the reconfiguration of the characteristic of elastic stability of the inlet. The system can be set to be bistable, super-elastic or simply stable.

Both experimental and theoretical results indicate the presence of a cusp singularity in the inlet's force versus displacement versus compression space, as well as its importance on the inlet's qualitative behaviour. Specifically, the cusp forms because the locus of snap-through and snap-back critical velocities and pressures coalesce as the panel compression is decreased. In general, the greater the applied compression, the higher the airspeed required to actuate the snap-through. For the design tested in this work, the critical snap-through velocities range between 26.7 and 40.3 $\mathrm{m\,s^{-1}}$. Conversely, snap-back can be seen only when the structure behaves super-elastically, with compression between 10.1 and 12.4×10^{-3}. Under these circumstances, the higher the degree of compression, the lower the airspeed to actuate snap-back. Given the generality of the underlying physical principle, the system's parameters can be tailored to fit specific operating conditions.

In conclusion, elastic instabilities have been exploited as a design tool to design a passively adaptive air inlet. The design framework proposed in this work facilitates the reconfiguration and control of stability and dynamic snap-through characteristics of the inlet, making the device suitable for a wide range of applications where shape adaptation and passive actuation are key, e.g. artificial valves and drug delivery in biomedical applications [26], NACA ducts in automotive and aerospace industries, and steering devices for sport yachts.

Future works will possibly include FSI simulations for the optimisation of the aerodynamic profile of the air inlet and a detailed study on the fatigue behaviour of the morphing component. In fact, the component is subjected to cyclic loads and large deformations. Although these do not induce sufficiently high strains to cause premature failure, they must be investigated in order to quantify the expected fatigue life. It is expected that fatigue will influence the design, but the good fatigue properties of composite materials, and preliminary tests conducted by the present authors in the order of a thousand cycles, suggest that the effect is expected to be small.

Acknowledgments

This work was supported by the UK Engineering and Physical Sciences Research Council (EPSRC) (grant no. EP/M013170/1 and no. EP/M507994/1), and the Royal Academy of Engineering under the Research Fellowship Scheme (grant no. RF/201718/17178). PMW acknowledges support of Science Foundation Ireland under its Research Professor scheme. We are also grateful to Clint Davies-Taylor and the SIMULIA UK technical team for their support.

Data statement

Data are available at the University of Bristol data repository, data.bris, at https://doi.org/10.5523/bris.3jn6y1fcr1zh22g0y95qtkjv4d.

ORCID iDs

G Arena https://orcid.org/0000-0002-4540-4071
R Theunissen https://orcid.org/0000-0001-5844-5158
P M Weaver https://orcid.org/0000-0002-1905-4477
A Pirrera https://orcid.org/0000-0003-3867-3916

References

[1] Wagg D, Bond I, Weaver P and Friswell M 2008 *Adaptive Structures: Engineering Applications* (New York: Wiley)
[2] Campanile L F 2005 Initial thoughts on weight penalty effects in shape-adaptable systems *J. Intell. Mater. Syst. Struct.* **16** 47–56
[3] Weisshaar T A 2013 Morphing aircraft systems: historical perspectives and future challenges *J. Aircr.* **50** (2) 337–53
[4] Sun J, Guan Q, Liu Y and Leng J 2016 Morphing aircraft based on smart materials and structures: a state-of-the-art review *J. Intell. Mater. Syst. Struct.* **27** 2289–312
[5] Brinkmeyer A, Pirrera A, Santer M and Weaver P 2013 Pseudo-bistable pre-stressed morphing composite panels *Int. J. Solids Struct.* **50** 1033–43
[6] Williams K, Chiu G and Bernhard R 2002 Adaptive-passive absorbers using shape-memory alloys *J. Sound Vib.* **249** 835–48
[7] Runkel F, Reber A, Molinari G, Arrieta A F and Ermanni P 2016 Passive twisting of composite beam structures by elastic instabilities *Composite Structures* **147** 274–85
[8] Valasek J 2012 *Morphing Aerospace Vehicles and Structures* vol 57 (New York: Wiley)
[9] Forterre Y, Skotheim J M, Dumais J and Mahadevan L 2005 How the Venus flytrap snaps *Nature* **433** 421–25
[10] Hu N and Burgueño R 2015 Buckling-induced smart applications: recent advances and trends *Smart Mater. Struct.* **24** 063001
[11] Poston T and Stewart I 1978 *Catastrophe Theory and its Applications* (New York: Dover Publications)
[12] Thompson J 1972 Optimization as a generator of structural instability *Int. J. Mech. Sci.* **14** 627–9
[13] Hunt G W 1977 Imperfection-sensitivity of semi-symmetric branching *Proc. R. Soc.* A **357** 193–211

[14] Daynes S, Potter K D and Weaver P M 2008 Bistable prestressed buckled laminates *Compos. Sci. Technol.* **68** 3431–7
[15] Daynes S, Weaver P M and Trevarthen J 2011 A morphing composite air inlet with multiple stable shapes *J. Intell. Mater. Syst. Struct.* **22** 961–73
[16] Gomez M, Moulton D E and Vella D 2017 Passive control of viscous flow via elastic snap-through *Phys. Rev. Lett.* **119** 144502
[17] Rothemund P, Ainla A, Belding L, Preston D J, Kurihara S, Suo Z and Whitesides G M 2018 A soft, bistable valve for autonomous control of soft actuators *Sci. Robot.* **3** eaar7986
[18] Arena G, Groh R M, Brinkmeyer A, Theunissen R, Weaver P M and Pirrera A 2017 Adaptive compliant structures for flow regulation *Proc. R. Soc.* A **473** 20170334
[19] Danso L A and Karpov E G 2017 Cusp singularity-based bistability criterion for geometrically nonlinear structures *Extreme Mech. Lett.* **13** 135–40
[20] Groh R and Pirrera A 2018 Generalised path-following for well-behaved nonlinear structures *Comput. Methods Appl. Mech. Eng.* **331** 394–426
[21] Timoshenko S P 1936 *Theory of Elastic Stability* ed S Timoshenko (New York: McGraw-Hill)
[22] Riks E 1979 An incremental approach to the solution of snapping and buckling problems *Int. J. Solids Struct.* **15** 529–51
[23] Ghidaoui M S, Zhao M, McInnis D A and Axworthy D H 2005 A review of water hammer theory and practice *Appl. Mech. Rev.* **58** 49–76
[24] Mallick P K 2007 *Fiber-Reinforced Composites: Materials, Manufacturing, and Design* (Boca Raton, FL: CRC Press)
[25] Zympeloudis E, Potter K, Weaver P M and Kim C B 2017 Advanced automated tape laying with fibre steering capability using continuous tow shearing mechanism *21st Int. Conf. on Composites Materials*
[26] Bavo A M, Rocatello G, Iannaccone F, Degroote J, Vierendeels J and Segers P 2016 Fluid-structure interaction simulation of prosthetic aortic valves: comparison between immersed boundary and arbitrary Lagrangian–Eulerian techniques for the mesh representation *PLoS One* **11** e0154517